WILEY-VCH

Supporting Information

Electric Field Effect in Co_3O_4/TiO_2 p-n Junction for Superior Lithium-Ion Storage

Huabin Kong, Chunshuang Yan, Chade Lv, Jian Pei, and Gang Chen**

MIIT Key Laboratory of Critical Materials Technology for New Energy Conversion and Storage
School of Chemistry and Chemical Engineering
Harbin Institute of Technology
Harbin 150001, P. R. China
E-mail: gchen@hit.edu.cn

Theoretical capacity calculation of P-Co_3O_4/TiO_2 NSs

The ICP results show the mass percent of Co and Ti are ~70.35% and 2.50% in P-Co_3O_4/TiO_2 NSs. The delithiation process can be described as:

$$Co_3O_4 + 8Li^+ + 6e \xrightarrow{\text{discharge}} 4Li_2O + 3Co$$

$$TiO_2 + xLi^+ + xe \xrightarrow{\text{discharge}} Li_xTiO_2$$

The theoretical capacity of P-Co_3O_4/TiO_2 NSs can be calculated by the following equations:

$$C = (F * n * 1000) / (t * M_w)$$

$$C_{(Co^{3+} \rightarrow Co^0)} = (96500 * 3 * 1000) * 70.35\%*(2/3) * / (3600 * 59)$$

$$= 639.2 \text{ mAh g}^{-1}$$

$$C_{(Co^{2+} \rightarrow Co^0)} = (96500 * 2 * 1000) * 70.35\%*(1/3) * / (3600 * 59)$$

$$= 213.1 \text{ mAh g}^{-1}$$

$$C_{(TiO_2 \rightarrow Li_xTiO_2)} = (96500*1*1000) * 2.50\%/ (3600 * 48) = 14.0 \text{ mAh g}^{-1}$$

$$C_{total} = 639.2 + 213.1 + 14.0 = 866.3 \text{ mAh g}^{-1}$$

Where F is the Faraday's constant, n is the valence charge, T is the time (in seconds), and M_w is the atomic mass. The calculated theoretical capacity of P-Co_3O_4/TiO_2 NSs is 866.3 mAh g^{-1}.

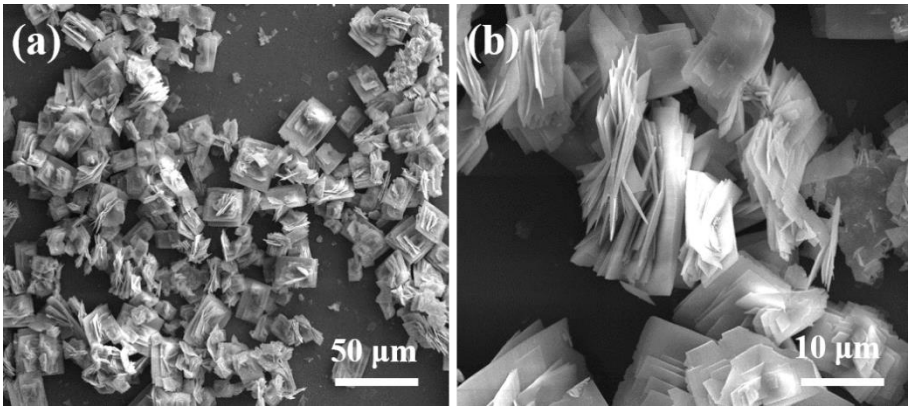

Fig. S1 (a, b) The SEM images of precursor.

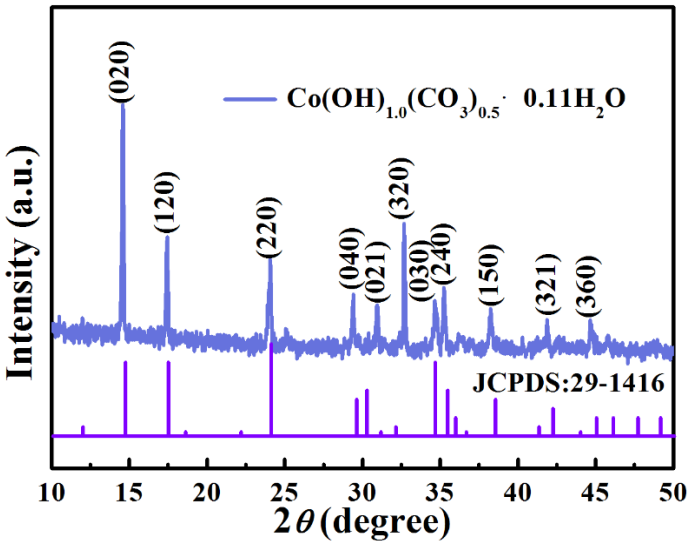

Fig. S2 The XRD pattern of precursor.

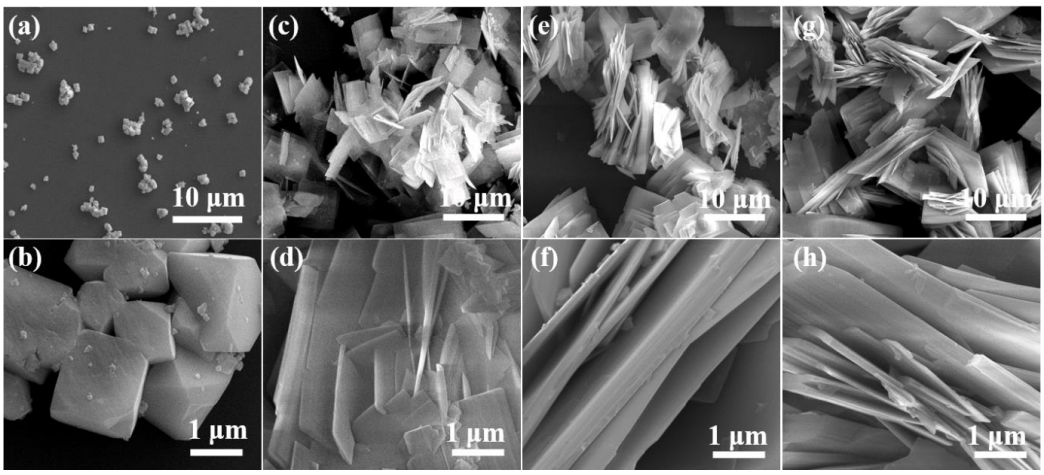

Fig. S3 The SEM images of the samples prepared under different urea content: (a, b) 0 g; (c, d) 0.25 g; (e, f) 0.5 g; (g, h) 0.75 g.

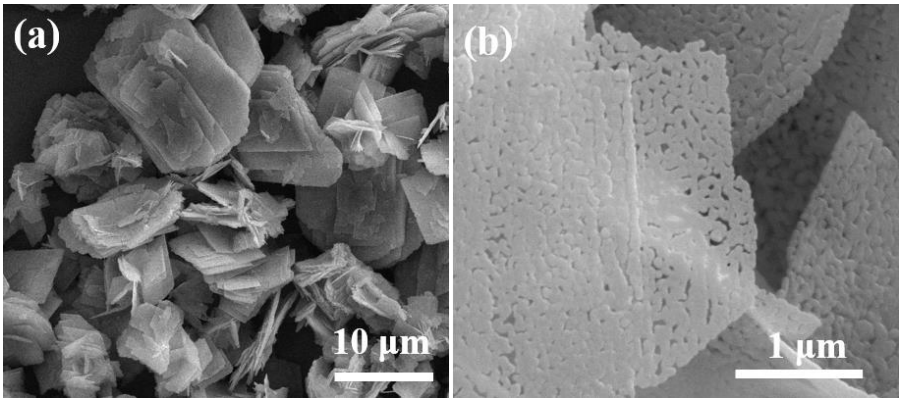

Fig. S4 (a, b) The SEM images of P-Co_3O_4 NSs.

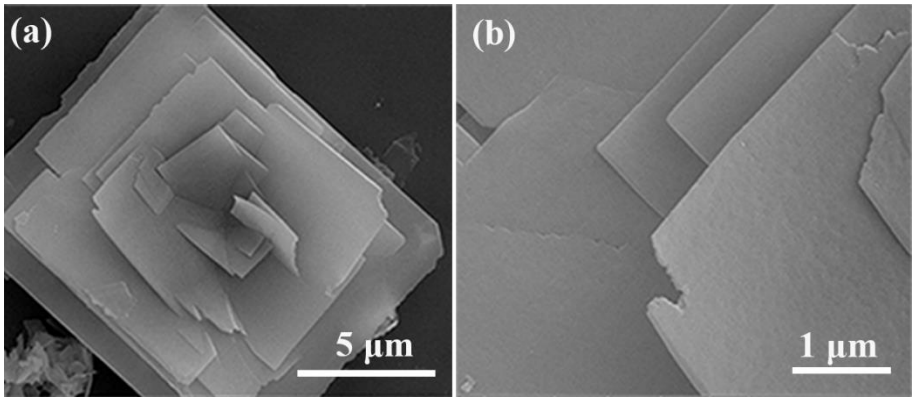

Fig. S5 (a, b) The SEM images of Co_3O_4 NSs.

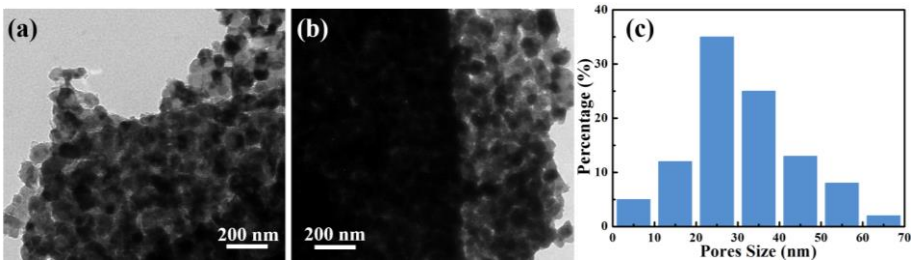

Fig. S6 (a, b) The TEM images of P-Co_3O_4/TiO_2 NSs, (c) the distribution of the pores size obtained by statistical analysis of the TEM images.

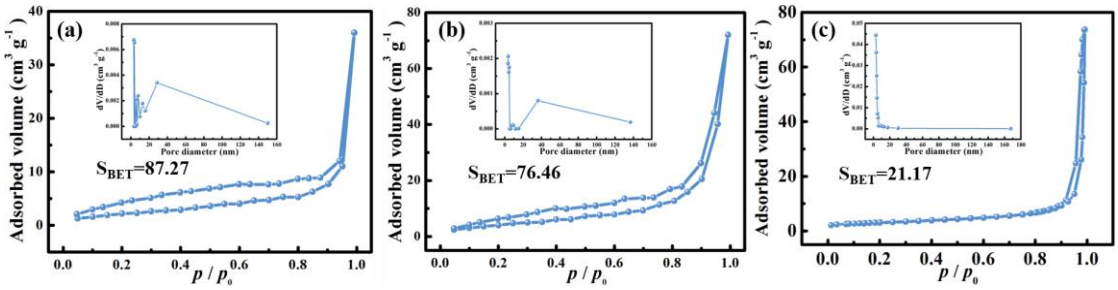

Fig. S7 Nitrogen adsorption/desorption isotherms and corresponding BJH pore size distributions (inset) of (a) P-Co_3O_4/TiO_2 NSs, (b) P-Co_3O_4 and (c) Co_3O_4.

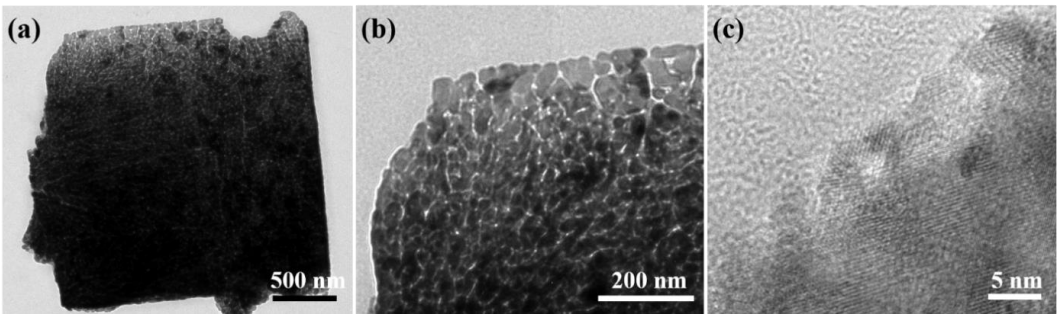

Fig. S8 (a, b) TEM images of P-Co_3O_4 NSs, (c) HRTEM image of P-Co_3O_4 NSs.

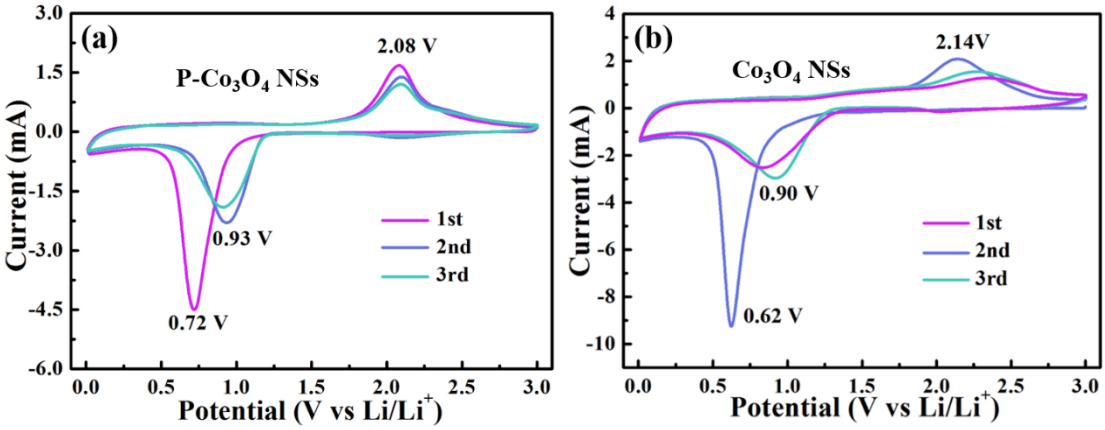

Fig. S9 (a, b) The CV curves of P-Co_3O_4 NSs and Co_3O_4 NSs in the first three cycles at a scan rate of 0.5 mV s^{-1}.

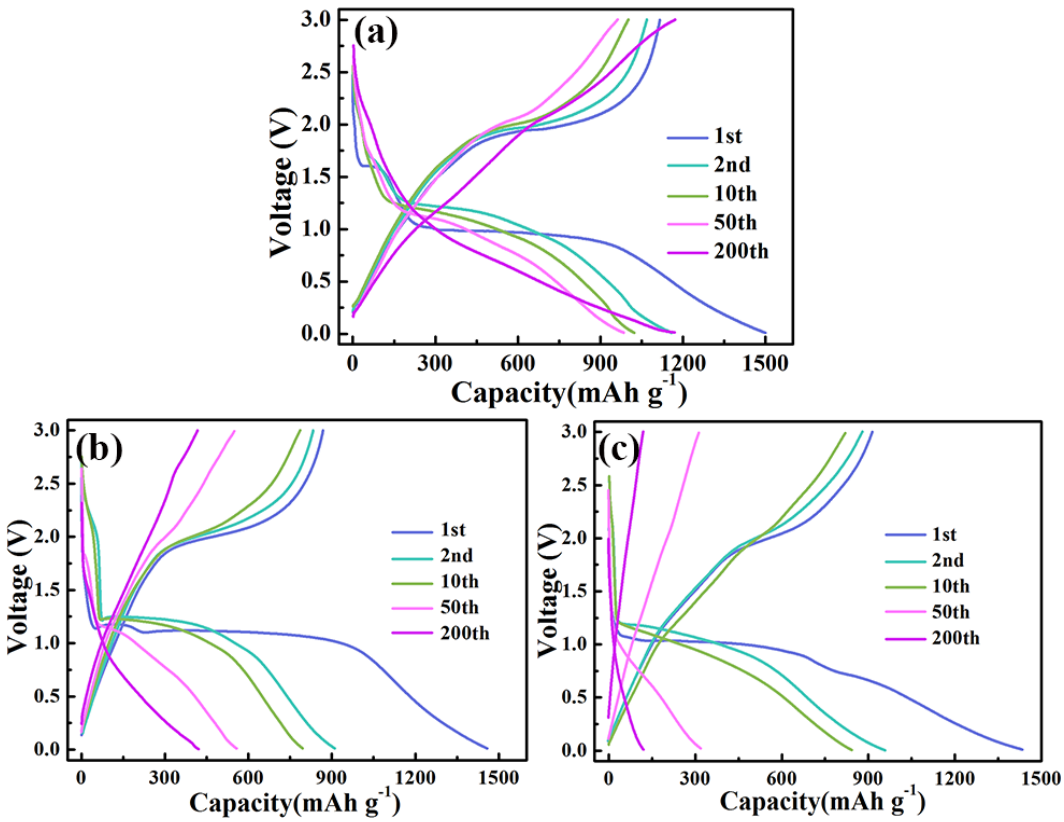

Fig. S10 (a, b, c) The charge/discharge profiles of P-Co_3O_4/TiO_2 NSs, P-Co_3O_4 NSs and Co_3O_4 NSs at a current density of 0.2 A g^{-1}.

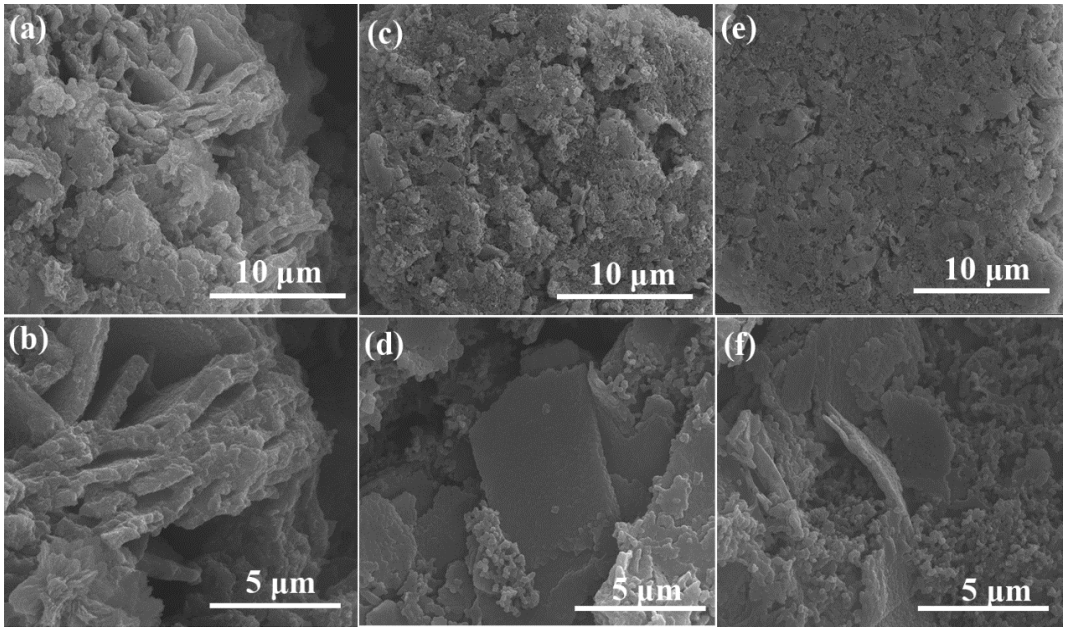

Fig. S11 The SEM images of the three electrodes after 200 cycles: (a, b) P-Co_3O_4/TiO_2 NSs, (c, d) P-Co_3O_4 NSs, (e, f) Co_3O_4 NSs.

Table S1 Performance comparison between P-Co_3O_4/TiO_2 NSs and previously reported Co_3O_4 nanosheets

LIB anode material	Current density ($mA\ g^{-1}$)	Cycle number	Capacity ($mAh\ g^{-1}$)
Porous Co_3O_4 nanoplates[1]	200	50	755
Co_3O_4 ultrathin porous nanosheets[2]	200	50	1053
Mesoporous Co_3O_4 nanosheet arrays[3]	1000	500	840
Co_3O_4–graphene sheet-on-sheet nanocomposite[4]	100	30	1065
2D holey Co_3O_4 nanosheets[5]	1000	200	1000
Three-dimensionally scaffolded Co_3O_4 nanosheet[6]	500	50	726
Mesoporous Co_3O_4 nanosheet/N-doped RGO[7]	80	50	1101
Porous Co_3O_4 nanoplates [8]	200	80	1001
Co_3O_4 nanobelts[9]	1000	60	614
Self-stacked Co_3O_4 nanosheets[10]	178	50	1070
Mesoporous hexagonal Co_3O_4[11]	1000	100	689
Ultrathin hexagonal Co_3O_4 nanosheets[12]	100	100	1007
This work	**200**	**200**	**1167**
This work	**2000**	**1600**	**801**

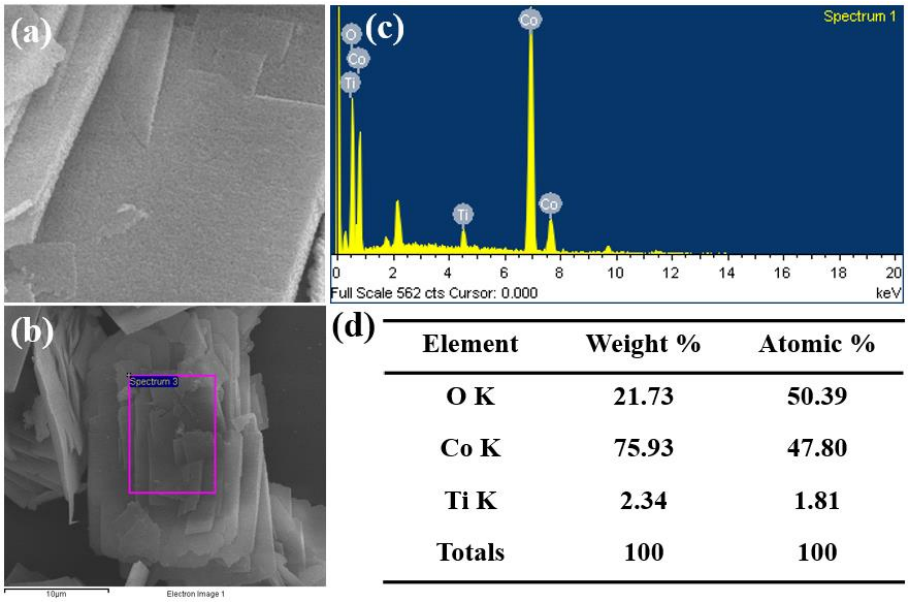

Element	Weight %	Atomic %
O K	21.73	50.39
Co K	75.93	47.80
Ti K	2.34	1.81
Totals	100	100

Fig. S12 (a, b) The SEM images of P-Co_3O_4/TiO_2 NSs, (c, d) the EDS result of P-Co_3O_4/TiO_2 NSs.

The SEM images of P-Co_3O_4/TiO_2 NSs are presented in Fig. S12a, b, which show a porous structure. The element contents of sample are analyzed by EDS (Fig. S12c, d), which shows the mass percent of Ti element is approximate to 2.34% in the P-Co_3O_4/TiO_2 NSs. The result of ICP shows the mass percent of Co and Ti is ~70.35.00% and 2.50%.

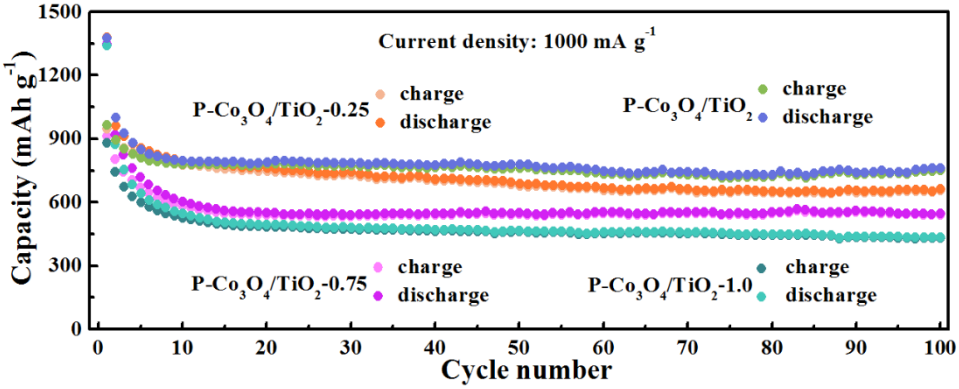

Fig. S13 Cycling performance of P-Co_3O_4/TiO_2-0.25 NSs, P-Co_3O_4/TiO_2 NSs, P-Co_3O_4/TiO_2-0.75 NSs and P-Co_3O_4/TiO_2-1.0 NSs at a current density of 1 A g^{-1}.

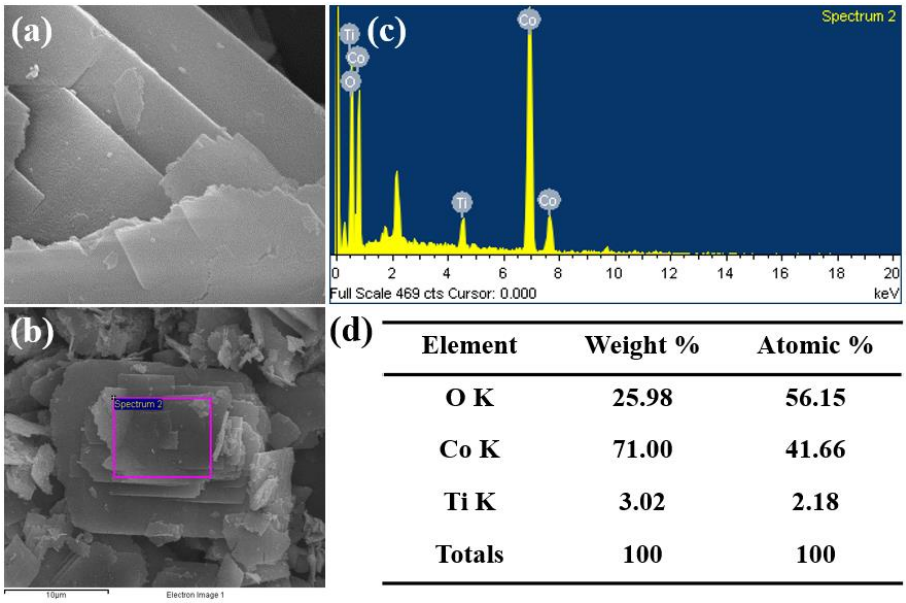

Element	Weight %	Atomic %
O K	25.98	56.15
Co K	71.00	41.66
Ti K	3.02	2.18
Totals	100	100

Fig. S14 (a, b) The SEM images of P-Co_3O_4/TiO_2-0.75 NSs, (c, d) the EDS result of P-Co_3O_4/TiO_2-0.75 NSs.

The SEM images of P-Co_3O_4/TiO_2-0.75 NSs are presented in Fig. S14a, b. When 0.75 ml titanium isopropanol is added, the morphology of P-Co_3O_4/TiO_2-0.75 NSs is similar to that of P-Co_3O_4/TiO_2 NSs, In addition, the element contents of sample are analyzed by EDS (Fig. S14c, d). The result shows the mass percent of Ti element is approximate to 3.02% in the P-Co_3O_4/TiO_2 -0.75 NSs.

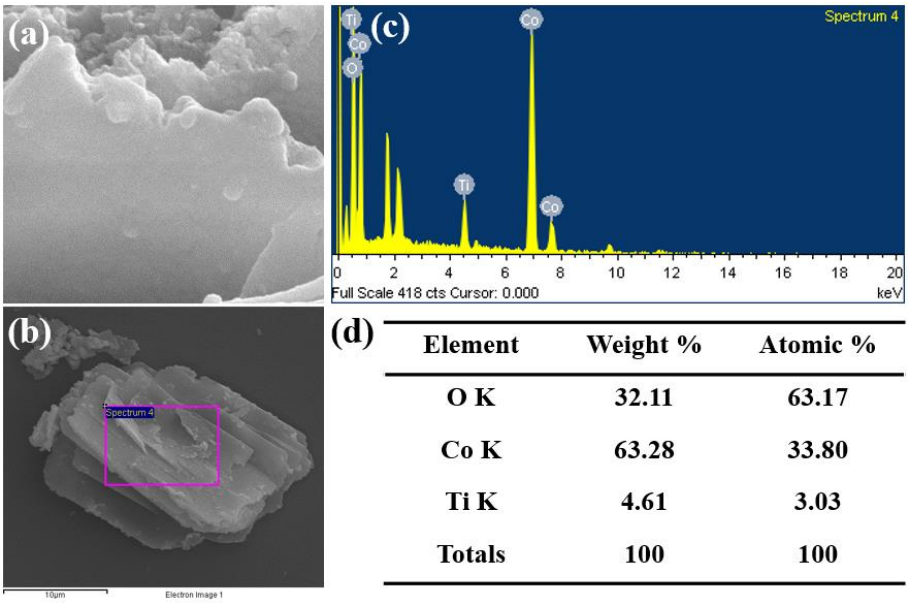

Element	Weight %	Atomic %
O K	32.11	63.17
Co K	63.28	33.80
Ti K	4.61	3.03
Totals	100	100

Fig. S15 (a, b) The SEM images of P-Co_3O_4/TiO_2-1.00 NSs, (c, d) the EDS result of P-Co_3O_4/TiO_2-1.00 NSs.

The SEM images of P-Co_3O_4/TiO_2-1.00 NSs are presented in Fig. S15a, b. When 1.00 ml titanium isopropanol is added, the omorphology of P-Co_3O_4/TiO_2-1.00 NSs is similar to that of P-Co_3O_4/TiO_2 NSs, In addition, the element contents of sample are analyzed by EDS (Fig. S15c, d). The result shows the mass percent of Ti element is approximate to 4.61% in the P-Co_3O_4/TiO_2 -1.00 NSs.

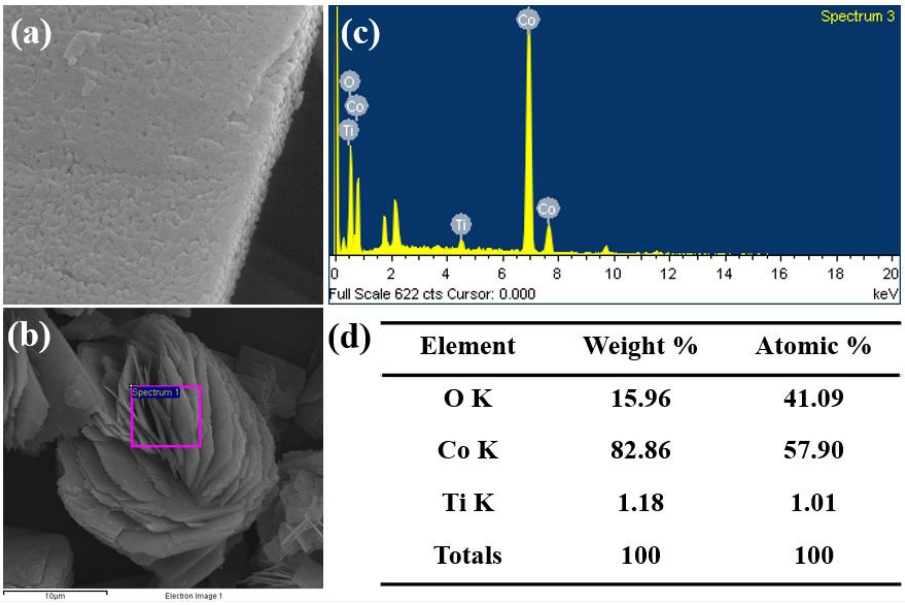

Element	Weight %	Atomic %
O K	15.96	41.09
Co K	82.86	57.90
Ti K	1.18	1.01
Totals	100	100

Fig. S16 (a, b) The SEM images of P-Co_3O_4/TiO_2-0.25 NSs, (c, d) the EDS result of P-Co_3O_4/TiO_2-0.25 NSs.

The SEM images of P-Co_3O_4/TiO_2-0.25 NSs are presented in Fig. S16a, b. When 0.25 ml titanium isopropanol is added, the morphology of P-Co_3O_4/TiO_2-0.25 NSs is similar to that of P-Co_3O_4/TiO_2 NSs, In addition, the element contents of sample are analyzed by EDS (Fig. S16c, d). The results shows the mass percent of Ti element is approximate to 1.18% in the P-Co_3O_4/TiO_2 -0.25 NSs.

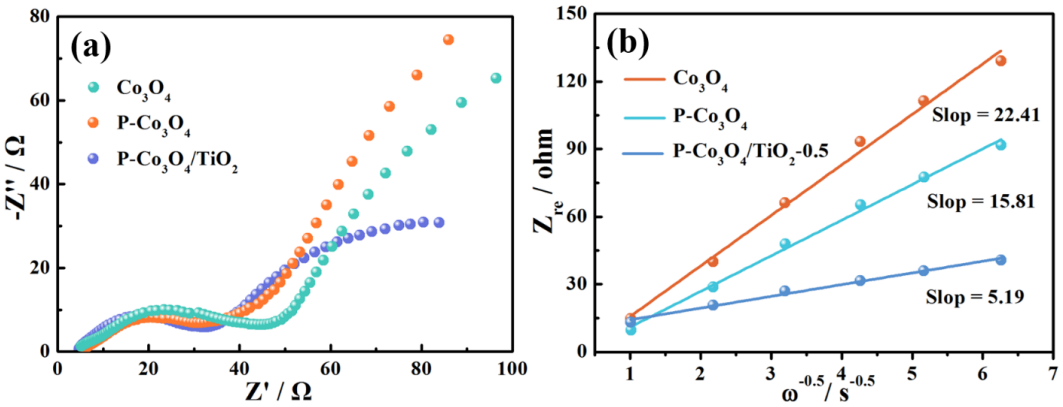

Fig. S17 Electrochemical measurement of electrodes made of the as-formed P-Co_3O_4/TiO_2 NSs, P-Co_3O_4 NSs and Co_3O_4 NSs, (a) Nyquist plots after 200 cycles, (b) The relationship between Z_{re} and $\omega^{-1/2}$ in the low frequency region.

The diffusion coefficient (D) of Li-ion can be calculated according to the following equation.[13]

$$Z_{re} = R_D + R_L + \sigma\omega^{-1/2} \quad (1)$$

$$D = 0.5(RT/An^2F^2C\sigma)^2 \quad (2)$$

Herein, R is the gas constant, A is the surface area, T is the absolute temperature, n is the number of electron per molecule oxidized, C is the concentration of Li-ion, F is the Faraday constant, σ is the Warburg impedance coefficient which is related to Z_{re}, ω is the angular frequency in the low frequency region, R_D and R_L are the diffusion resistance and liquid resistance, respectively. The slopes of the fitting curve in Figure S17b are Warburg impedance coefficient σ. It is shown that the Warburg impedance coefficient of P-Co_3O_4/TiO_2 NSs, P-Co_3O_4 NSs and Co_3O_4 NSs are 5.19, 15.81 and 22.41 Ω cm^2 $s^{-1/2}$, respectively. According to equation 2, the D value of P-Co_3O_4/TiO_2 NSs is higher than P-Co_3O_4 NSs and Co_3O_4 NSs, indicating that p-n junction is benefit to accelerate the Li-ion diffusion.

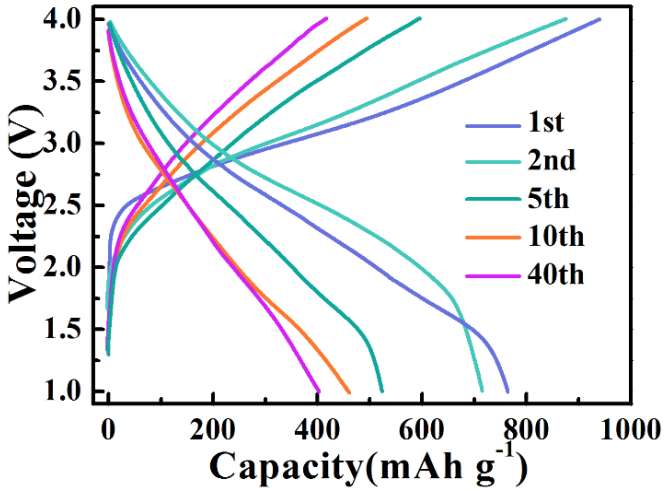

Fig. S18 The charge/discharge profiles of full cell (anode: P-Co_3O_4/TiO_2 NSs//cathode: commercial $LiNiCoMnO_2$) at a current density of 0.1 A g^{-1}.

References

1 Q. Su, J. Zhang, Y. Wu, G. Du, *Nano Energy*, 2014, **9**, 264–272.
2 J. Mujtaba, H. Sun, G. Huang, Y. K. Mølhave, Y. Liu, Y. Zhao, X. Wang, S. Xu, J. Zhu, *Sci. Rep.*, 2016, **6**, 20592.
3 X. Fan, Y. Shi, L. Gou, D. Li, *Electrochim. Acta.*, 2014, **142**, 268–275.
4 S. Chen, Y. Wang, *J. Mater. Chem.*, 2010, **20**, 9735–9739.
5 D. Chen, L. Peng, Y. Yuan, Y. Zhu, Z. Fang, C. Yan, G. Chen, JR. S. Yassar, L. Lu, K. Amine, G. Yu, *Nano Lett.*, 2017, **17**, 3907–3913.
6 J. Liu, S. J. Kelly, E. S. Epstein, Z. Pan, X. Huang, J. Liu, P. V. Braun, *J. Power Sources.*, 2015, **299**, 40–48.
7 P. Sennu, H. S. Kim, J. Y. An, V. Aravindan, Y. S. Lee, *Chem. Asian J.*, 2015, **10**, 1776–1783.
8 C. Liang, D. Cheng, S. Ding, P. Zhao, M. Zhao, X. Song, F. Wang, *J. Power Sources.*, 2014, **251**, 351–356.
9 H. Huang, W. Zhu, X. Tao, Y. Xia, Z. Yu, J. Fang, Y. Gan, W. Zhang, *ACS Appl. Mater. Interfaces*, 2012, **4**, 5974–5980
10 X. Wang, H. Guan, S. Chen, H. Li, T. Zhai, D. Tang, Y. Bando, D. Golberg, *Chem. Commun.*, 2011, **47**, 12280–12282.
11 D. Su, X. Xie, P. Munroe, S. Dou, G. Wang, *Sci. Rep.*, 2014, **4**, 6519.
12 B. Wang, X. Lu, Y. Tang, W. Ben, *ChemElectroChem.*, 2016, **3**, 55–65.
13 Y. Cui, X. Zhao, R. Guo, *Electrochim. Acta*, 2010, **55**, 922–926.
14 Q. Wang, Y. Huang, J. Miao, *Electrochim. Acta*, 2013, **93**, 120–130.